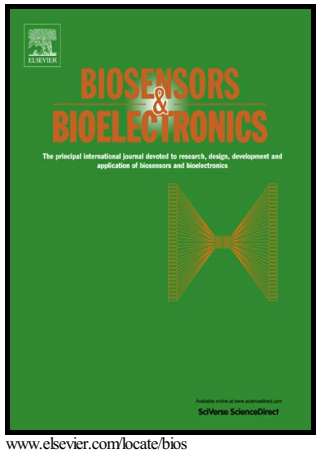

www.elsevier.com/locate/bios

ScFv-modified Graphene-coated IDE-arrays for 'label-free' screening of cardiovascular disease biomarkers in physiological saline

Lotta E. Delle, Vivek Pachauri, Shikha Sharma, Olena Shaforost, Hui Ma, Mohammad Adabi, Rainer Lilischkis, Patrick Wagner, Ronald Thoelen, Norbert Klein, Richard O'Kennedy, Sven Ingebrandt

PII: S0956-5663(17)30801-1
DOI: https://doi.org/10.1016/j.bios.2017.12.005
Reference: BIOS10150

To appear in: *Biosensors and Bioelectronic*

Received date: 13 September 2017
Revised date: 4 December 2017
Accepted date: 5 December 2017

Cite this article as: Lotta E. Delle, Vivek Pachauri, Shikha Sharma, Olena Shaforost, Hui Ma, Mohammad Adabi, Rainer Lilischkis, Patrick Wagner, Ronald Thoelen, Norbert Klein, Richard O'Kennedy and Sven Ingebrandt, ScFv-modified Graphene-coated IDE-arrays for 'label-free' screening of cardiovascular disease biomarkers in physiological saline, *Biosensors and Bioelectronic,* https://doi.org/10.1016/j.bios.2017.12.005

ScFv-modified Graphene-coated IDE-arrays for 'label-free' screening of cardiovascular disease biomarkers in physiological saline

Lotta E. Delle[1], Vivek Pachauri*[1], Shikha Sharma[2], Olena Shaforost[3], Hui Ma[2], Mohammad Adabi[3], Rainer Lilischkis[1], Patrick Wagner[4], Ronald Thoelen[5], Norbert Klein[3], Richard O'Kennedy[2], Sven Ingebrandt[1]

Author's affiliations:

1. Department of Informatics and Microsystem Technology,
   University of Applied Sciences Kaiserslautern,
   Amerikastraße 10, 66482 Zweibrücken, Germany

2. School of Biotechnology
   Dublin City University,
   Glasnevin, Dublin 9, Ireland

3. Department of Materials,
   Imperial College London,
   South Kensington, London SW7 2AZ, United Kingdom

4. Soft-Matter Physics and Biophysics Section
   Department of Physics and Astronomy,
   Catholic University Leuven, Celestijnenlaan 200d, 3001 Leuven, Belgium

5. Institute for Materials Research,
   Hasselt University,
   Wetenschapspark 1, 3590 Diepenbeek, Belgium

Corresponding author: pachauri.vivek@gmail.com; vivek.pachauri@hs-kl.de

KEYWORDS: scFV, Graphene, Biosensor, Cardiovascular, Electrical sensing, Physiological buffer

Abstract

Fatty-acid binding proteins (FABP) and myeloperoxidases (MPO) are associated with many chronic conditions in humans and considered to be important biomarkers for diagnosis of cardiac diseases.

Here we assemble a new electrical biosensor platform based on graphene-coated interdigitated electrode arrays (IDE-arrays) towards ultrafast, label-free screening of heart type-FABP and MPO. Arrays of nanoscale (nanoIDE) and microscale (microIDE) electrode-arrays were fabricated on wafer-scale by combining nanoimprint and photolithography processes. Chemical vapor deposition grown multilayer graphene was transferred onto nano/microIDE-arrays and used as a high surface-to-volume ratio electrical transducer. Novel biofunctional layers of specially engineered anti-h-FABP and anti-MPO single-chain fragment variables (scFv) were immobilized onto graphene-coated IDE-array sensor platform for electrical detection of h-FABP and MPO in physiological saline. scFv fragments show increased sensitivity in comparison to the state-of-the-art competitive ELISA for their higher affinity towards target analytes. Deploying FABP and MPO specific scFvs as receptor molecules onto our high-sensitivity graphene-coated IDE-arrays with identical sensor characteristics and assays covering clinically relevant concentrations in physiological saline, we demonstrate realization of a simple and versatile biosensor platform capable of high performance cardiac-bioassays for point-of-care applications.

Graphical abstract:

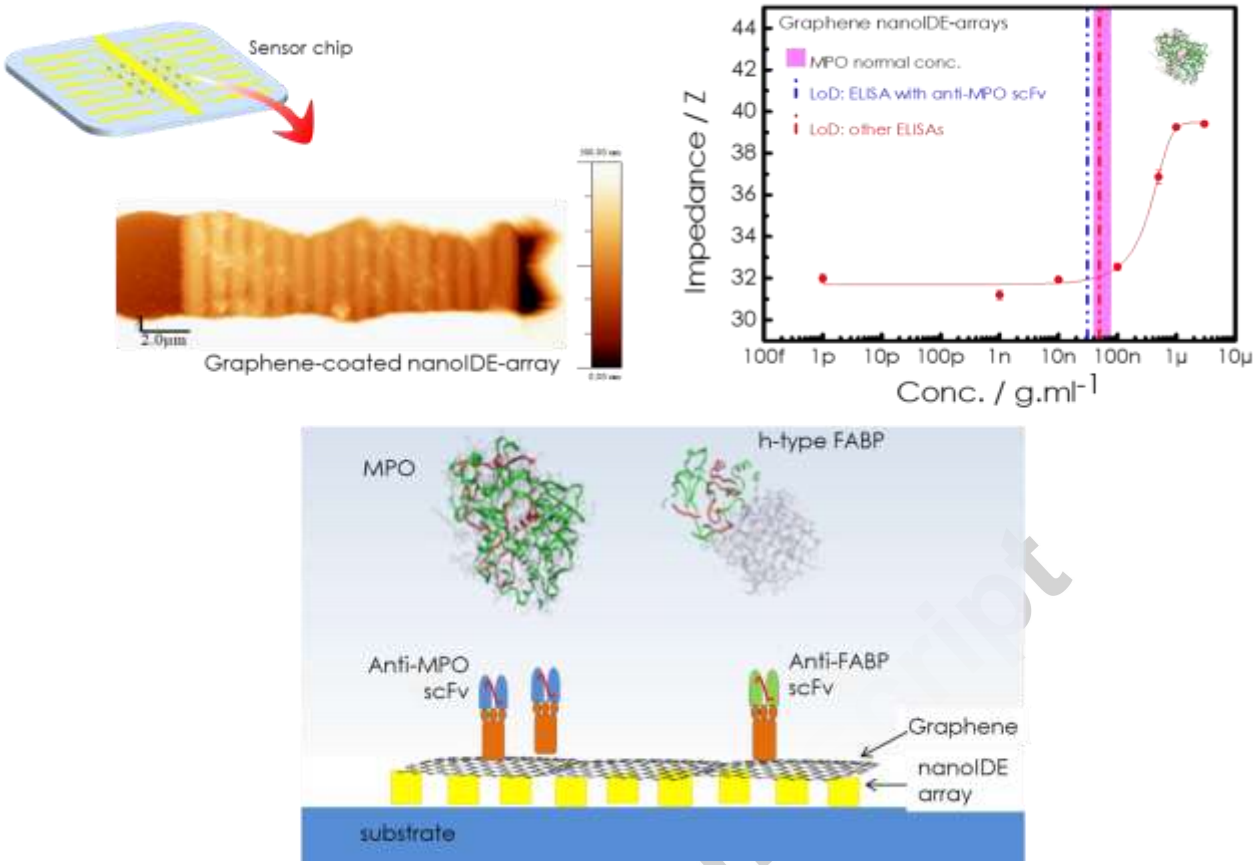

1. Introduction

According to recent surveys, cardiovascular diseases (CVDs) remain a leading cause of mortality in human populations worldwide.(Balakumar et al. 2016) With equal shares from coronary problems and heart strokes, over 17 million CVD-related deaths account for about 30 percent of the total number of deaths. CVD related deaths are more prevalent in populations with low and mid-level incomes across the globe making up to three quarters of total CVD-related deaths. By number, CVDs are one of the leading causes of deaths in high income groups as well. Overall, CVD-related diseases are significant burden on healthcare systems across the globe.(Wilkins et al. 2017) In combating CVDs, risk stratification and diagnosis of cardiovascular conditions has evolved significantly and help accomplish major therapeutic findings over the last years.(Steg et al. 2012) Even though, prediction models for the CVDs and medical interventions remain dependent on demographic study of physical symptoms such as diet, smoking, life-style, level of cholesterol and prevalence of diabetes. It should

be noted that up to 20 percent of CVD patients may not identify with such prediction models.(Hozawa et al. 2007) Addressing the shortcomings of concurrent models, efforts are being concerted towards the discovery of molecular biomarkers and their inclusion in disease prediction, stratification models for high-risk (with high incidences of traditional risk symptoms) as well as low-risk patients (with little or no symptoms before the onset of the disease). As a molecular basis to cardiovascular diseases, biomarkers such as C-reactive proteins (CRP), h-type fatty acid binding proteins (FABP), Growth-differentiation factor-15, pregnancy-associated plasma protein-A (PAPP-A), highly sensitive troponin (hTp), heart-type myeloperoxidase (MPO), B- type natriuretic peptide (BNP) and its deriative, N-terminal natriuretic peptide (NT-proBNP) have been associated to various pathophysiological processes.(Wang et al. 2017) Diagnosing a panel of such biomarkers is therefore very interesting for health-care, which may allow identification of specific conditions such as myocardial injury, inflammation, plaque formation/rupture, myocardial abnormalities, platelets or neuro-hormonal activation and serve as a basis to develop future therapeutic strategies and drug-discoveries.(Chatterjee and Singh 2015; Fang 2015; Savic-Radojevic et al. 2017; Wang et al. 2017) Out of numerous CVD biomarkers identified in recent years, studies have shown that detection of h-FABP alone or along with hTp is far superior for rapid diagnosis of acute myocardial infractions.(Azzazy et al. 2006; Kaczynska et al. 2006; Liang et al. 2011; Lippi et al. 2013; Otaki et al. 2014) Similarly, increased levels of MPO are closely associated with coronary artery diseases (CAD) and are found to be more efficient as biomarker.(Baldus et al. 2003; Nicholls et al. 2011) Superior attributes of FABP and MPO as biomarkers make them ideal candidates for realization of efficient sensor platform in prognosis of cardiovascular problems.

Uses of such molecular biomarkers for clinical assays demand realization of high-performance sensor platforms in biological or physiological media where low concentration levels and varying clinically relevant ranges pose significant challenges for reliable screening. Here, state-of-the-art optical detection techniques used for screening purposes mostly perform on the borderline and require a performance boost. Consequently, alternative strategies towards the development of more efficient bioassays are most sought-after. For example, realizations of high-sensitivity micro-/nano-

electrochemical transducers as miniaturized point-of-care (PoC) platforms are converging with optical approaches towards overcoming challenges of future medical diagnostics.(Bellan et al. 2011; Connolly 1995; Pickup 1985) In parallel, use of specially engineered bioreceptors such as aptamers, single chain fragment variables (scFv) with high specificity and affinity towards target analytes are allowing unique solutions to improve the performance of biosensor platforms.(Ayyar et al. 2010; Holliger and Hudson 2005; Huston et al. 1988; Ma and O'Kennedy 2017). A scFv consists of variable regions of heavy and light-chain immunoglobulin domains joined by a peptide link, considerably smaller than their antibody counterparts.(Schroeder et al. 1998) scFv-antibodies have become part of the established practices for synthesis of immunotoxins, anticancer intrabodies. Therapeutic gene delivery and cancer-treatment are opening up new possibilities for scFv in medical diagnosis and control.(Ahmad et al. 2012; Spain et al. 2016) Other than their use for optical bioassays, scFv are especially interesting for assembly of label-free electrical biosensors where performances are governed by the solid-liquid interface, characterized by low receptor-analyte affinities and formation of very thin electrical double layers due to high ionic strengths.(Daniels 2007) Among other solutions, use of bioreceptors with smaller molecular sizes and high-affinities e.g. scFv are expected to compensate for such performance limitations in electrical biosensors.

In this work, we present a new electrochemical sensor platform based on the use of graphene as a nanomaterial transducer combined with newly designed scFv as the biofunctional layer for efficient label-free detection of h-type FABP and MPO. For the assembly of biosensor platform, graphene was grown in a chemical vapor deposition process and transferred on to nanoscale interdigitated electrode arrays (nanoIDE-arrays) and microscale interdigitated electrode arrays (microIDE-arrays). Graphene surfaces were further modified with anti-fatty acid binding protein (anti-FABP) or anti-myeloperoxidase (anti-MPO) scFv for the detection of h-FABP and MPO, respectively. Superior affinity binding of the newly designed anti-MPO and anti-FABP scFv were tested by inhibitory concentration (IC50) analysis using competitive enzyme-linked immunosorbent assays (ELISA) and showed improved sensor performances compared to similar state-of-the-art assays. The electrical biosensors were integrated in a 16 channel, fluidic-chip design to form a miniaturized biosensor

platform. With this sensor approach we deploy 'label-free' impedimetric detection of biomarker analytes (FABP and MPO) in concentration ranges spanning $pg.ml^{-1}$ to $\mu g.ml^{-1}$ in physiological saline. Our scFv-modified, graphene-coated IDE-arrays exhibit sensor dynamic ranges covering clinically relevant concentrations of analytes with extremely reliable sensor signals across different sensor positions on a chip. The use of high-sensitivity and reliable screening platforms based on scFv modified graphene-IDE based transducers such as presented in our work are expected to ideally serve as a generic pathway for further development of low-cost, clinical assays for CVD biomarkers. Assembly of such miniaturized PoC tools with further optimizations in patient's samples is highly advantageous for accessing reliable information on the prognosis of CVDs to inform timely interventions and prevention of fatal conditions in high risk patients.(Damen et al. 2016)

2. Materials and Methods

2.1. scFv production: h-FABP and MPO specific receptor scFv proteins were produced after extracting specific RNA sequences from the host animals followed by reverse transcription and production of scFv protein libraries. The production of these libraries and subsequent steps using phase display technology for the selection of highly specific scFv, purification procedure, SDS-PAGE analysis and expression is discussed in the supporting information (SI1-SI4).

2.2. Competitive ELISA: Half-area 96-well plates (Fisher, Ireland) were coated with 30 µL of 2.5 µg/mL hFABP and 2 µg/mL MPO (AMS Biotechnologies, UK) separately and left overnight at 4°C. The plates were then blocked by using 60 µL/well of 5% (w/v) PBSTM at 37°C for one hour, followed with a wash using PBS (60 µL/well). To carry out the competitive ELISA, different concentrations of hFABP (0-500 $ng.ml^{-1}$) or MPO (0-2,000 ng/mL) were prepared and mixed with a fixed concentration of anti-hFABP (0.26 µg/mL) and anti-MPO (0.03 µg/mL) scFv. This mixture (30µL/well) was incubated at room temperature for 10 min and served for the competitive ELISA measurements. For performance of negative control experiments, 30 µL/well of hFABP-free and MPO-free human serum were applied instead of the scFv and antigen mixture. The plates were washed using PBS (60 µL/well) followed with addition of HRP-labelled HA antibody (1:1,000 dilution; 30 µL/well) and incubation at room temperature for 10 min. The plates were washed once

again using PBS (60µL/well). TMB in what (0.4 g/L, 30µL/well) was added to the plates and incubated at room temperature for 2 min. The reaction was stopped by addition of 30 µL of 1 M HCl per well. The absorbance of the wells was read at 450 nm using a Safire 2 plate reader.

2.3. Wafer-scale nanofabrication of sensor chips and graphene transfer: The sensor chips with nanoIDE and microIDE-arrays were fabricated in newly developed top-down lithography on Si/SiO_2 wafers approach with combination of nanoimprint and lithography processes. The process flow of the nanofabrication process and further details are given in the supporting information (SI5). The graphene layers were grown in a chemical vapor deposition (CVD) process over 2" x 2" copper foils. The graphene transfer onto the sensor chips was carried out using a solution-based process with polystyrene as a polymer support.(Yu et al. 2014) In brief, graphene covered copper foils were coated with polystyrene film and cut into small sizes (approx. 3 x 3 mm) which was sufficient to cover all the 16 nanoIDE or microIDE-array channels on the sensor chips. To prepare the polymer film, typically a polystyrene bead weighing around 0.07 grams was dissolved in 3 ml toluene (procured from Sigma Aldrich, Germany) and drop casted on top of the graphene-coated copper foil. The polymer-coated graphene foils were baked for 5 minutes in a convection oven at 95 °C. Polystyrene-coated foils were carefully transferred to a copper etching bath made up of 2.5 ml H_2O_2, 7.5 ml HCl (both Sigma Aldrich, Germany) and 42 ml deionized water. Foils are left floating on the solution surface for copper etching resulting in polystyrene films with graphene layer sticking underneath. The graphene layer with the polystyrene film on top was transferred to a water bath for cleaning and then fished out by placing sensor chips under the floating graphene layer in appropriate orientation so as to cover the nanoIDE or microIDE-arrays. After immobilizing the polystyrene-coated graphene onto the sensor areas, the sensor chips were placed in toluene solution for 2 hours on a shaker to wash off the polystyrene layer from the graphene. Before graphene transfer, sensor chips were cleaned using ultrasonication in acetone, isopropanol and distilled water (5 min each) and subsequently by plasma cleaning in an oxygen plasma chamber (Diener Electronic, Germany) at 0.6 mbar, 140 Watts for 5 min. After graphene transfer, the sensor chips were annealed at 350°C for 2 h in an argon atmosphere.

2.4. Structural, electrical characterization and sensor integration: Topographical characterization of the sensor chips was carried out using scanning electron microscopy (Zeiss Supra 40 SEM, Carl Zeiss AG), atomic force microscopy (Nanoscope Dimension 3100 AFM, Veeco probes, USA) and Raman microscopy (Horiba LabRam spectrometer). Field-effect characterization of sensor chips was carried out on a semiconductor parameter analyzer (Keithley 4200-SCS, Tektronix, USA), while impedimetric measurements for transconductance measurements and determination of cut-off frequency were carried out using a home built, 16 channel portable amplifier for dc and ac measurements. For the realization of biosensor platform and measurements, sensor chips were wire-bonded onto PCBs and encapsulated using a borosilicate glass ring (borosilicate glass 3.3, d_o: 9 mm, d_i: 7 mm, wall thickness: 1 mm, h: 2 mm, from Becker Glas, Germany) and using a PDMS (Sylgard 184, Dow Corning USA) layer. This glass ring is glued onto the sensor chip surrounding the sensor arrays while a larger glass ring (borosilicate glass 3.3, d_o: 20 mm, wall thickness: 1.2 mm, d_i: 17.6 mm, h: 3 mm, Becker Glass, Germany) was placed concentrically and covered the wire-bonds connecting the sensor chip with the electrical contact pads of the PCB. The space between the glass rings, which also protected the wire-bonds was filled with PDMS and cured in an oven at 120 °C. With this encapsulation procedure, the gold bonds were completely passivated by PDMS and a small reservoir on top of the sensor area was assembled for easy placement of analyte solutions during analytical measurements. Encapsulated sensor chips were placed onto a plastic-lead chip carrier (PLCC 68 1.27 mm pitch T+B IC51, Yamaichi electronics, Japan) equipped with wire connections addressing channels on the sensor chip, individually.

2.5. Realization of biofunctional layers and sensor measurements: For bioimmobilization of anti-FABP and anti-MPO scFv recombinant antibody fragments on graphene-coated nanoIDE and microIDE-arrays, sensor chips were treated with 95% 3-mercaptopropyltrimethoxysilane (MPTMS) from Sigma Aldrich, Germany in propanol (1:100 ratio). 40 microliter (µl) MPTMS solution was placed on the sensor chip for 2 hours, cleaned with propanol-2, and blow-dried with N_2 gas. Forty microliter solutions of anti-FABP scFv and anti-MPO scFv at 1µg/ml concentrations were placed on the sensor surface and incubated for ~12 hours. After incubation, the immobilization solution was

discarded and the sensor surface was rinsed twice with PBS, pH 7.4. Detection of FABP and MPO was carried out with concentration ranges of 1 $pg.ml^{-1}$ – 1 $\mu g.ml^{-1}$ and 1 $pg.ml^{-1}$ – 3 $\mu g.ml^{-1}$, respectively with an incubation of 10 min for each concentration using a sample volume of 400 µl. For label-free detection of h-type FABP and MPO in physiological saline, non-faradaic electrochemical impedance spectroscopy (EIS) measurements were carried out. (Daniels 2007) An electrochemical workstation Zahner Zennium from Zahner-elektrik GmbH & Co. KG, Germany was used for performing EIS. The operation of sensor platform using EIS is similar to as discussed in a previous report by our group.(Lanche et al. 2015)

3. Results and Discussion

The assembly of the graphene-based sensor platform is illustrated in **figure 1**. The IDE-arrays working as *source* and *drain* electrodes were fabricated on 4-inch Si/SiO_2 wafers using a top-down lithography approach combining nanoimprint lithography and photolithography methods. Figures 1a and 1b show scanning electron microscopy (SEM) images of the typical nanoIDE-arrays and microIDE-arrays on the sensor chips. NanoIDE-arrays and microIDE-arrays with finger width of 600 nm and 6 µm were separated with 600 nm and 6 micron interdigital gaps, respectively. Each sensor chip contained 16 of these source-drain pairs containing well defined nanoIDE-arrays and microIDE-arrays with regular interdigital source-drain gaps working eventually as an '*electrical channel'* or *'transducers'* after graphene transfer. The source-drain pairs were surface passivated with a 450 nm thick passivation layer (SiO_2-Si_3N_4-SiO_2) in the contact-line regions in order to minimize interactions with the analytes as well as to define the transducer area, as can be clearly seen in the SEM scan images 1a and 1b. The solution-mediated CVD graphene transfer process is illustrated in figure 1C, which employed polystyrene as a support for graphene. In order to ascertain the detailed topographical features of the graphene-coated nanoIDE-array and microIDE-array sensor platforms, the sensor chips were characterized by atomic force microscopy (AFM) and Raman microscopy techniques. Figure 2 shows the surface characterization of typical sensor chips and subsequently, the surface modified, graphene-coated IDE-arrays with anti-MPO and anti-FAB scFv as biofunctional layers. Figure 2a shows an AFM image of a typical nanoIDE-array coated with graphene. The graphene layer can be clearly seen to completely cover the nanoIDE-array while extending onto the passivation layer. Graphene transfer on the passivated electrode array therefore limits the transducer area to the passivation window and consequently helps to minimize device-to-device variation in sensor characteristics. A zoomed in AFM scan image on the right side shows the transducer area and the nanoIDE-array covered with graphene. A further illustration on surface characterization of graphene-coated sensor platform is shown in supporting information SI6. The thickness of the graphene layer was determined after transferring them onto flat silicon substrates as shown in supporting information (SI7) and measured to be around 8 to 10 nm corresponding to 10 to 15

layers.(Shearer et al. 2016) The thickness of the graphene layers was measured. Figure 2b shows the Raman microscopic characterization of the graphene layer directly on the sensor platform (inset image). The graph shown in the image represents a typical Raman spectrum for multilayered graphene.(Ferrari and Basko 2013) The higher G-band intensities (1565 cm^{-1}), presence of a faint D peak (1132 cm^{-1}) and a low intensity 2D peak (2670 cm^{-1}) can be attributed to a disordered lattice, defects and folding of multilayers during the growth or transfer process.(Cong and Yu 2014; Das et al. 2008; Ferrari and Basko 2013; Park and Ryu 2015) G-peak intensity for the multilayer Graphene transferred onto the nanoIDE-array is shown in the optical image as figure 2b. The inhomogeneous spatial distribution of the intensity may be due to the folding of graphene multilayers. The graphene-coated IDE-arrays were then functionalized with either anti-MPO or anti-FABP scFv as receptor molecules. The schematics shown in figure 2c and 2d illustrate realization of the biofunctional layers. The immobilization process details are given in the methods section. Figure 2e shows the AFM image of a sample device after biofunctionalization. As compared to the graphene-coated IDE-arrays in shown in figure 2a, the antibody fragment scan be clearly seen in the AFM image, distributed over the graphene layer forming granular and agglomerated structures. A comparison of typical sensor position before and after carrying out the bioimmobilization procedure is shown in supporting information (SI9). The assembled sensor platform was mounted on a specially designed polymer circuit board (PCB) and integrated with a fluidic reservoir on top to carry out the electrical bioassays.

It is worth take a note of the significant surge in label-free electrical biosensor concepts based on one-dimensional (1D) and two-dimensional (2D) transducers exhibiting superlative sensor performances.(Balasubramanian and Kern 2014; Pachauri 2016; Rani et al. 2016) Implementation of such nanoscale sensor platform for real applications; however, requires overcoming several technological and economic thresholds. Here, inabilities to mass produce identical nanomaterial transducers, biomaterials for sensor integration and challenges in detection of clinically relevant analyte concentrations in highly concentrated buffers remain major concerns.(Biju 2014; Hinchet and Kim 2015) While discovery of highly-sensitive, versatile nanomaterial transducers and developments in top-down nanofabrication approaches are mitigating reproducibility issues, realization of high-

performance biofunctional layers has often been overlooked. Optimal design and function of receptor biomolecules is a critical aspect in deploying direct label-free sensor concepts and demand special attention towards developing real applications.(Baker 2015; Daniels 2007; Oliveira Jr. et al. 2014) Engineering of high-affinity biomolecular interfaces here becomes crucial to develop highly efficient biomolecular assays.(Lee et al. 2008; Luo and Davis 2013; O'Sullivan 2002)

In order to ascertain the analyte binding performance of scFv anti-MPO and anti-FABP, a standard half maximal inhibitory concentration analysis (IC50) was carried out using an ELISA protocol. IC50 measurements were carried out by competing immobilised anti-FABP and anti-MPO scFv with solution-phase FABP and MPO are shown in figures 3a and 3b. The binding activity was evaluated by the IC50: the concentration at which half-maximum inhibition of antibody-antigen interactions by the competing antigen is achieved. With the indirect competition ELISA, the obtained values of IC50 for anti-hFABP and anti-MPO scFv were approximately 16 and 500 ng/mL, respectively. The limit of detection (LoD) for anti-hFABP and the anti-MPO scFv were approximately 2 and 31 $ng.ml^{-1}$, respectively. The results suggested that although the ELISA with scFv give better sensitivities than their regular counterparts (80 and 50 $ng.ml^{-1}$ for FABP and MPO, respectively), LoD remain within or just below the healthy ranges of FABP (1-30 $ng.ml^{-1}$) and MPO (40-80 $ng.ml^{-1}$).(Esporcatte et al. 2007; Goiffon et al. 2015; Ishimura et al. 2013; Mocatta et al. 2007; Otaki et al. 2014; Wodzigl et al. 1997)

After the ELISA-based analysis of scFv recombinant proteins, electrical bioassays were carried out using the graphene-coated nanoIDE-arrays. Figure 4 shows the assembled sensor platform and measurements carried out for ‘label-free’ sensing of FABP and MPO in a buffer solution with physiological salt concentrations (phosphate buffer with an ionic strength of 154 mM). Figure 4a and 4b show photographs of the complete sensor system, where the sensor chip is mounted on to a PCB, encapsulated with a fluidic reservoir, and connected to external electrical contacts. For sensing experiments, an alternating current (AC) bias was applied between the source and drain electrodes against a reference which is provided by an Ag/AgCl reference electrode mounted at a fixed position in the center of the fluidic reservoir. Source and Drain IDEs are connected by the transducer graphene

layer causing an electrical resistance (R_G). Total impedance (Z) of devices is recorded in order to carry out impedimetric sensing of FABP and MPO. Six different concentrations of FABP (1 pg.ml^{-1}, 500 pg.ml^{-1}, 1 ng.ml-1, 10 ng.ml-1, 100 ng.ml^{-1} and 1 µg/ml^{-1}) and 7 different concentrations of MPO (1 pg.ml^{-1}, 1 ng.ml^{-1}, 10 ng.ml^{-1}, 100 ng.ml^{-1}, 500 ng.ml^{-1}, 1 µg/ml^{-1} and 3 µg/ml^{-1}) were prepared in the high ionic strength phosphate buffer to use as sample solutions. Impedance of the scFv-modified graphene-coated IDE-array chips was measured after pipetting 400 µl sample solution for each of the concentrations and after incubation for 10 minutes. Figure 4c and 4d show the impedance behavior of anti-FABP scFv-modified graphene-coated nanoIDEs-based and microIDEs-based sensor chips, respectively. Measurements were performed by applying a sinusoidal perturbation potential of 100 mV rms vs. the open circuit potential in a frequency range from 1 Hz-10 kHz between the source and drain IDE-array contacts lines. The impedance behavior of the sensor chips clearly shows a consistent increase of impedance with increasing concentration of MPO. It is interesting to note that the impedance behavior of the graphene-nanoIDE-arrays was significantly different towards the higher frequencies (> 3 kHz) as compared to graphene-microIDE-arrays, which may be due to higher capacitive load in the nanoscale sensors. Differential transfer function measurements of graphene-coated nanoIDE-arrays and microIDE-arrays against a frequency modulated electrochemical bias carried out in different ionic strengths also showed higher frequency cut-offs for graphene-coated nanoIDE-arrays (supporting information SI10). The impedance behavior of the anti-MPO-modified graphene-coated nanoIDE-arrays and microIDE-arrays upon introducing different concentrations of MPO is shown in figures 4e and 4f. The impedance behavior was recorded for frequencies ranging from 1Hz to 10kHz, showing consistent increase in the impedance with increase of MPO concentrations. It is to be noticed that although the device-to-device variation in impedance values on a sensor chip were near-identical (figure 5), the graphs in the figure 4 show measurements of devices from different chips resulting in variations in impedance values may be coming from slight differences in the graphene transfer and cleaning processes during the assembly of sensor platform.

Figure 5 summarizes the biosensor response of graphene-coated nanoIDE-arrays and microIDE-arrays and compares the performance of our electrical bioassays with the classical ELISA-based approaches.

All the graphs from 5a to 5d show average impedance values from 16 individual channels on a sensor chip recorded at 30 Hz (red dots connected with red dashed line). The pink background represents tentative FABP and MPO biomarker concentrations of clinical relevance in humans on the x-axis, while the red and blue dash-dot vertical lines show LoD values for conventional ELISA based protocols reported in literature and ELISA screening with scFV, respectively. The graphene-coated IDE sensors showed a wide dynamic range from $pg.ml^{-1}$ to $\mu g.ml^{-1}$ concentrations, with a sigmoidal dose response curve for both MPO and FABP biomarkers. The limit-of-detection for graphene-coated nanoIDE-array and microIDE-array platforms for FABP, MPO was calculated using linear regression analysis in low concentration ranges, respectively at 300 $pg.ml^{-1}$, 112 $pg.ml^{-1}$ and 158 $ng.ml^{-1}$ and 350 $pg.ml^{-1}$. As it can be seen from the graphs shown in figure 5, the sensors showed promising performance with the FABP assay demonstrating an almost linear response in the clinically-relevant concentration range for the micro-IDE sensors. A comparison with other sensor platform reported in literature so far shows superlative performance of our sensor platform yielding one of the shortest assay-time of approximately 10 min. and able to detect most wide spread of FABP, MPO concentrations (Supporting information SI12). For real clinical applications however, a further improvement of our sensor platform is needed. Especially, the relatively small clinically relevant concentration range for MPO requires an optimized resolution in this range, where the nanoIDE sensor might have the best potential to meet this demand (see figure 5c). Graphene-coated nanoIDE-arrays without biofunctionalization were used for negative control of the bioassays developed here for the detection of FABP and MPO in physiological saline which is shown in the supporting information (SI11).

Conclusion

In this manuscript, we present a new electrical biosensor platform provided by fabrication of nanoscale and microscale IDE-arrays using top-down nanoimprint lithography and photolithography methods and, subsequently, transferring graphene as a 2D transducer material. The graphene-coated nanoIDE and microIDE-array-based devices were surface factionalized with scFv recombinant antibody fragments for efficient binding of FABP and MPO, important cardiovascular disease

biomarkers. The assembled sensor platform showed high-performance sensor characteristics with very low device-to-device variations. Most importantly, sensors were deployable in physiological buffers for 'label-free' screening of large protein molecules such as FABP and MPO. Limitations of optical and other sensing approaches in detection of very low concertation of such biomarkers in complex media is a significant challenge to overcome in order to realize 'point-of-care' platforms for clinical diagnostics. Wide sensor dynamic ranges beyond clinically relevant concentration ranges demonstrated by our sensor platform together with low LoD at $pg.ml^{-1}$ concentrations of FABP and MPO in physiological buffers are expected to provide a significant thrust in the development of electrical assays for clinical applications. Our sensor approach is expected to aid in the development of further healthcare diagnostic solutions in high-risk patients suffering from cardiovascular patients as well as enable the realization of personalized diagnostics platforms for regular health monitoring

Acknowledgements

We thank Prof. K. Balasubramanian for the help with the solution mediated graphene transfer process. This research work was supported by the Stiftung Rheinland-Pfalz für Innovation Nr. 1082.Vivek Pachauri acknowledges the support from Euroimmun AG for funding of his position. We also acknowledge support from European Commission FP7 Programme through the Marie Curie Initial Training Network PROSENSE (grant no. 317420, 2012-2016) and from DCU INVENT and Imperial sources). All the authors thank Detlev Cassel, Andreas Pastille and Walid Munief for their help in the clean-room processes and with the surface characterizations.

Figures:

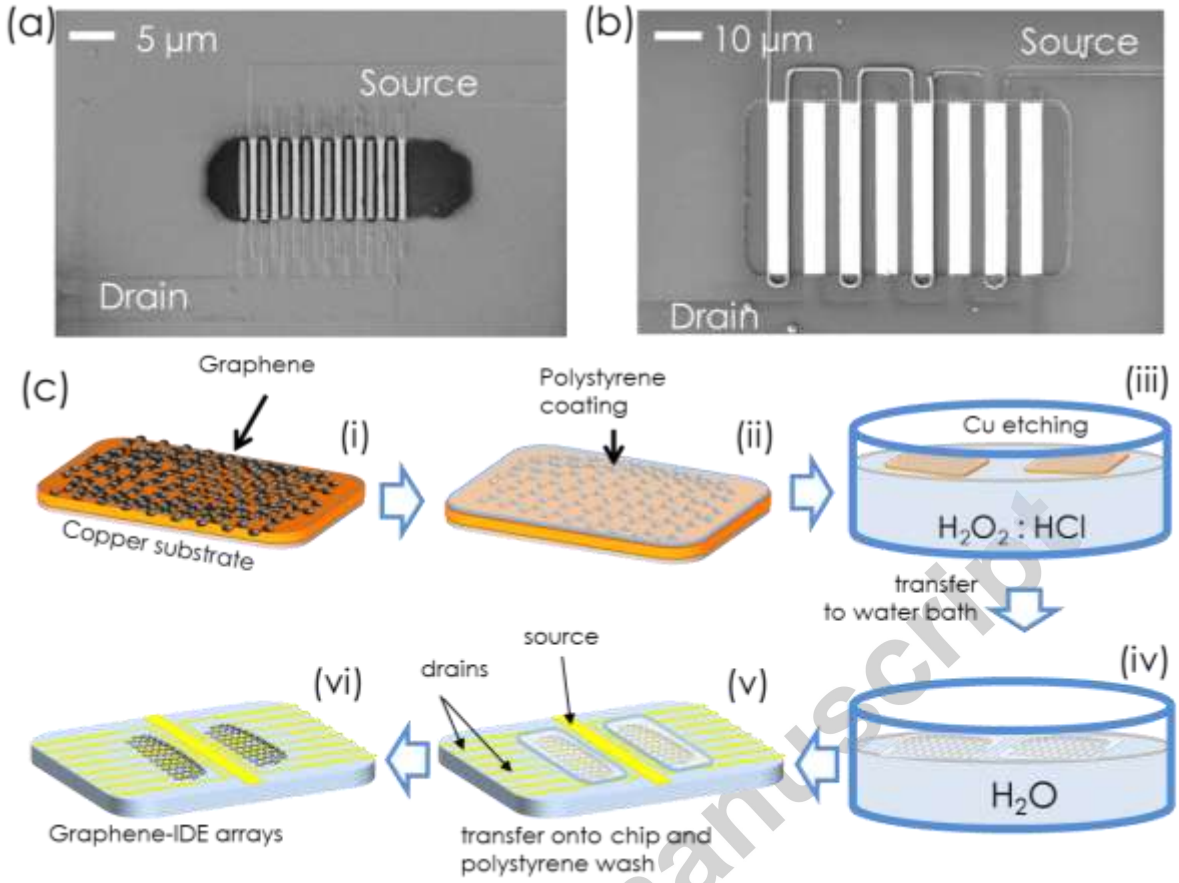

Figure 1: Preparation of graphene-coated nanoIDE and microIDE-array sensor chips. (a) SEM image of a nanoIDE-array chip showing 16 nanoelectrodes with a passivation layer protecting the electrode contacts. (b) SEM scan image of the microIDE-arrays chip showing 8 microelectrodes with a passivation layer. (c) Schematic illustration of the solution-based graphene transfer process from the copper substrate onto the sensor chips using polystyrene support.

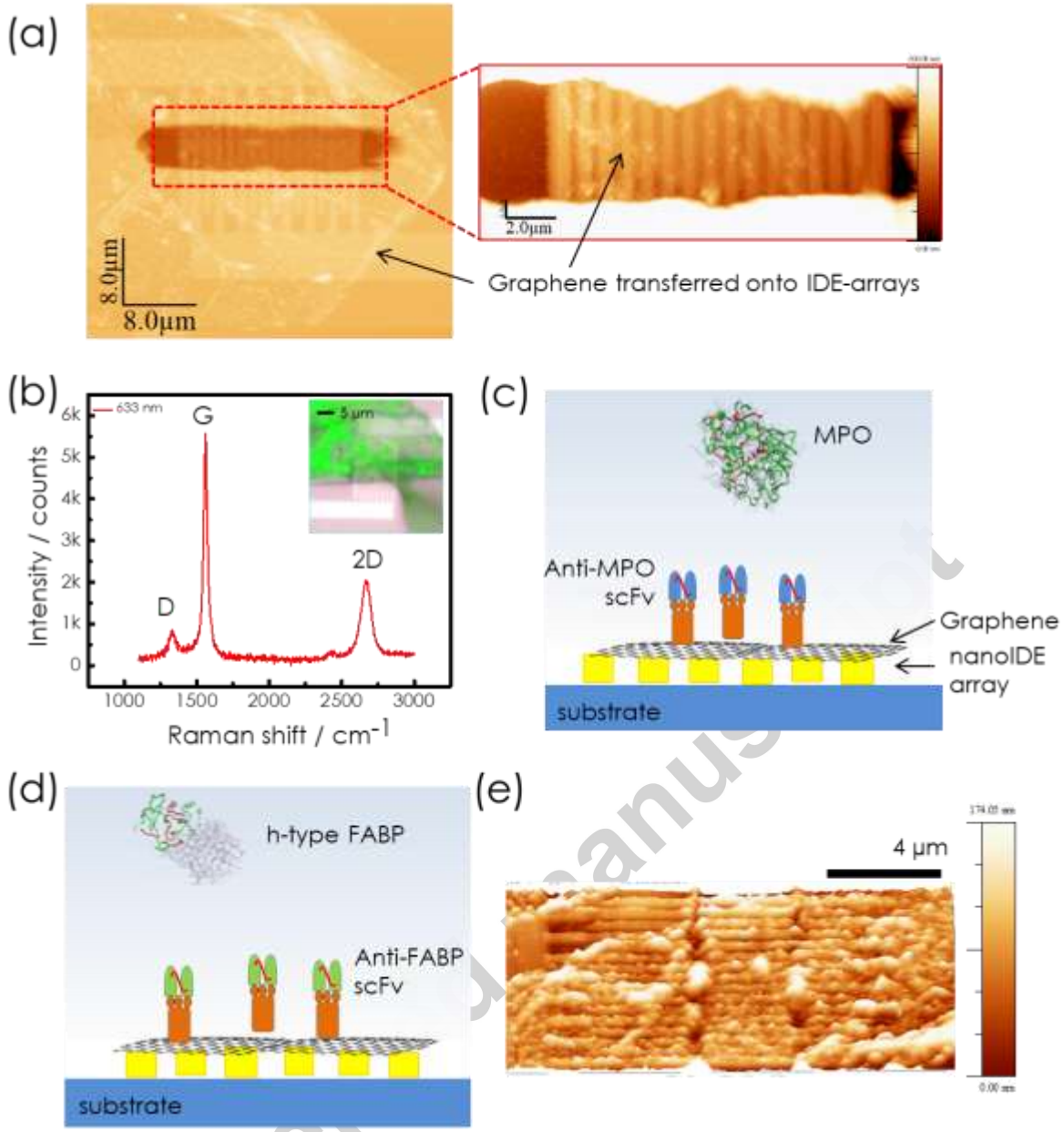

Figure 2: Characterization of the graphene-coated IDE-arrays and assembly of the sensor platform. (a) Atomic force microscopy image of a nanoIDE-array after positioning graphene on top showing a complete coverage of the nanoelectrodes with the graphene layer. (b) The graph shows a typical Raman spectrum of the graphene layer positions on top of nanoIDE-array. The image in the inset represents a characteristic Raman map taken over the sensor-area, whereas the green overlay - represents the G-peak intensities of the graphene layer. (c, d) Schematic illustration of the bioimmobilization of multilayer graphene-coated IDE-arrays chips with anti-MPO and anti-FABP scFv recombinant antibodies, respectively. (e) AFM image of a typical sensor surface after the bioimmobilization process.

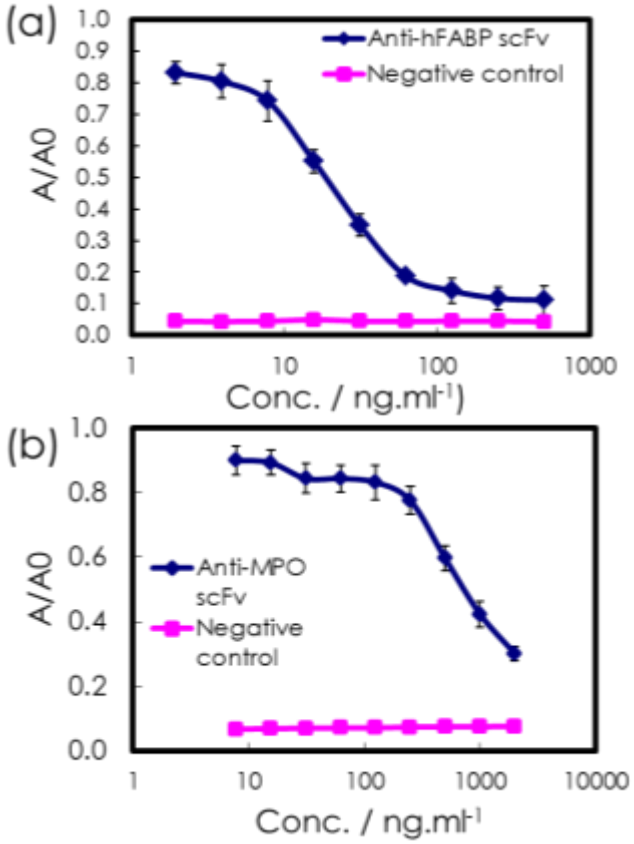

Figure 3: Competitive ELISA showing the limit of detection using (a) anti h-FABP and (b) anti-MPO scFv antibody fragments proteins. Absorbance with no h-FABP or MPO competition is referred to as A0. The absorbance with h-FABP and MPO competition are referred to as A. For the negative control, the absorbance with h-FABP-free and MPO-free sera was used instead of A/A0. The results are shown as the mean ± S.D. (n=3).

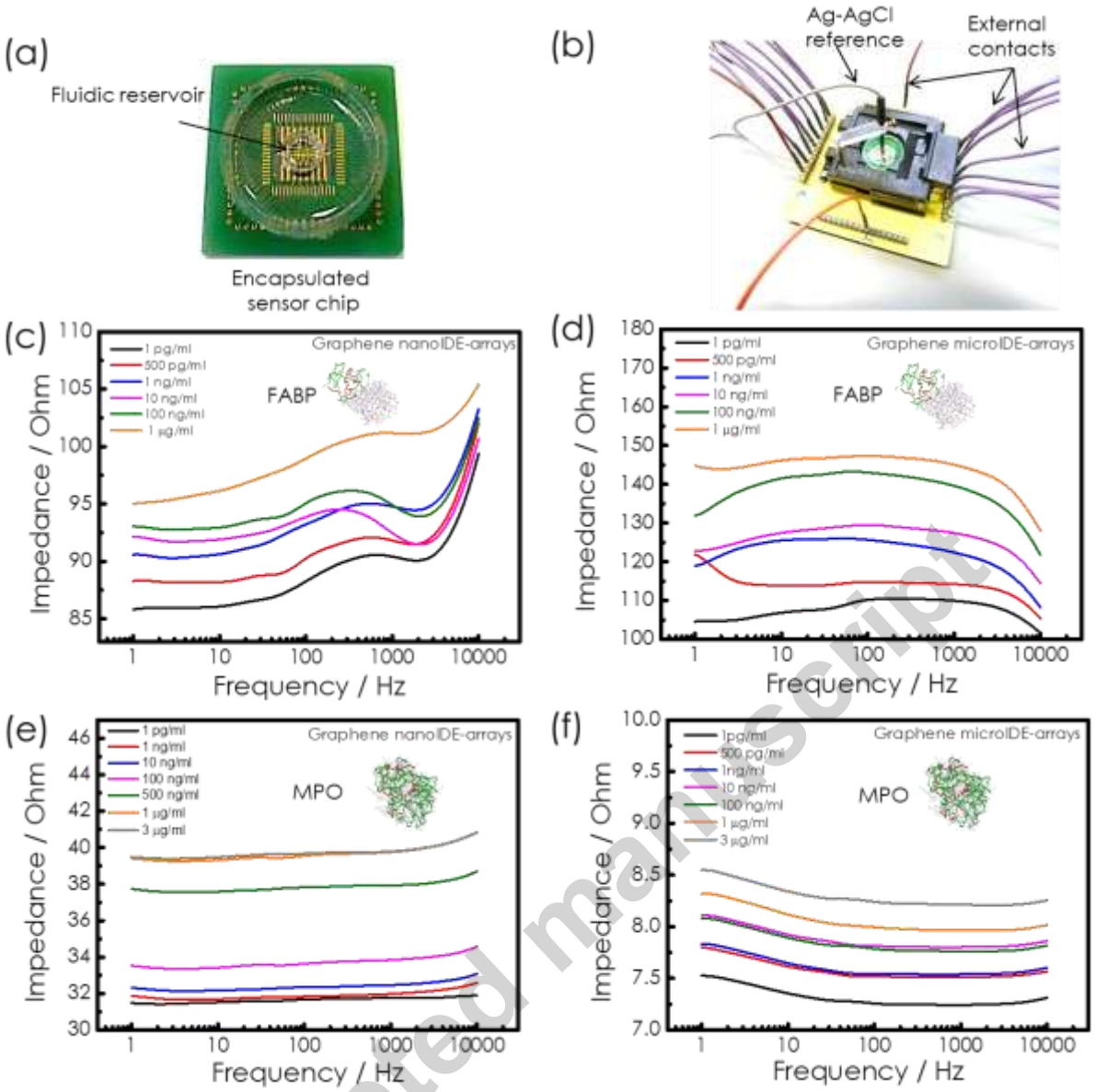

Figure 4: Label-free screening of cardiac disease biomarkers on graphene-coated IDE-arrays. (a, b) The encapsulated sensor chip and the measurement set-up is shown in the photograph, where a sensor-chip is assembled on top of a chip-carrier, encapsulated with a fluidic chamber and connected to external electrical contacts for measurements. An individual sensor chip is shown in the inset. (c, d) In-line impedance spectra of the sensor chips (graphene-coated nanoIDE and microIDE-arrays, respectively) biofunctionalized with anti h-FABP scFv when subjected to different concentrations of h-type FABP in physiological buffer. (e, f) In-line impedance spectra measured for different concentrations of MPO in physiological buffer on the anti-MPO scFv-modified sensor chips.

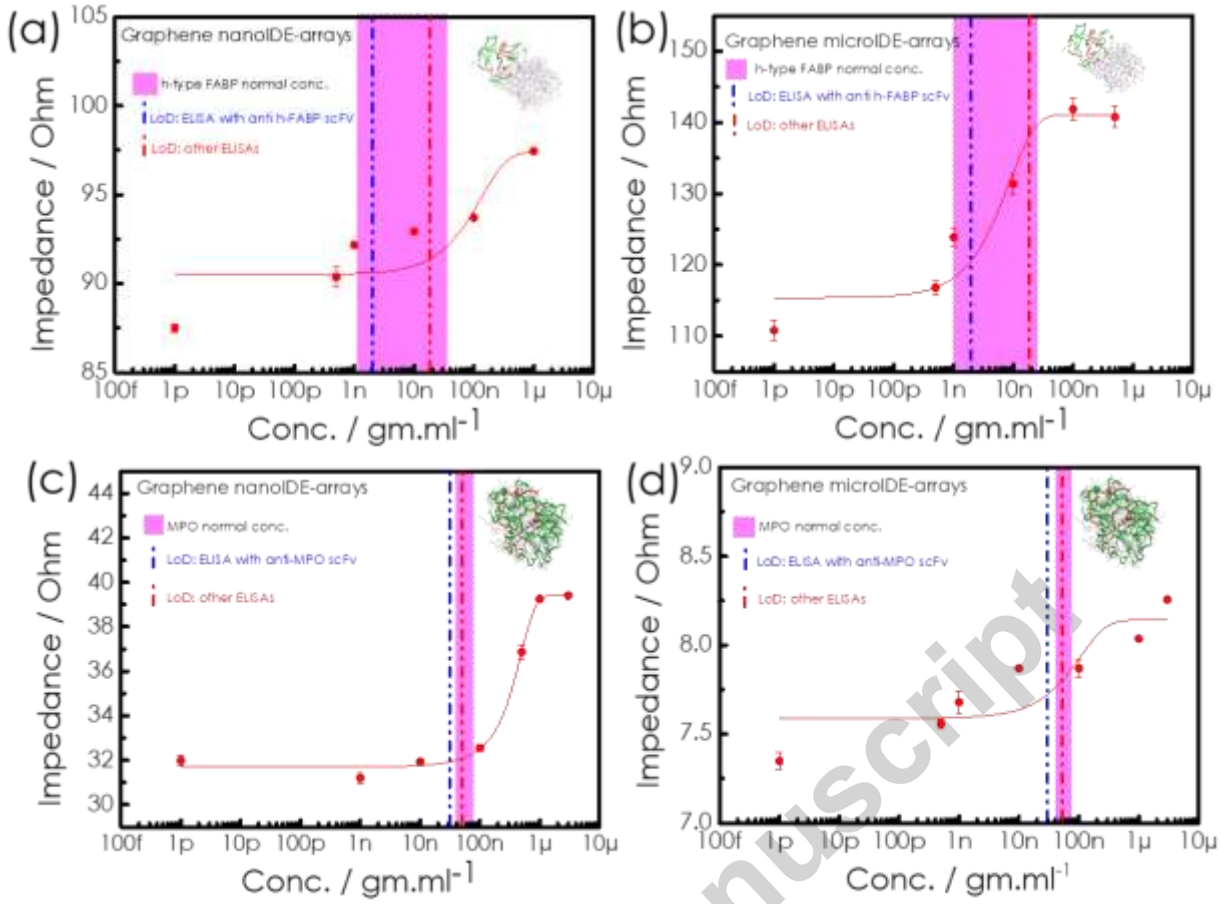

Figure 5: Performances of graphene-coated IDE-arrays sensor platform vis-à-vis ELISA methods for the detection of h-type FABP and MPO. (a) The graph showing a nearly sigmoidal increase in the impedance values (extracted at 30 Hz) of the graphene-coated nanoIDE-array sensors as a function of h-type FABP concentration in the buffer shown as red dots and a dashed line extrapolated in red color. The purple box shows the normal concentration of h-type FABP in humans while the red and blue vertical dash-dot lines show the LoD using state-of-the-art ELISA methods and ELISA procedure using scFv recombinant antibody fragments as used in this study, respectively. (b) Dose-response curve obtained for different h-type FABP concentrations in buffer using graphene-coated microIDE-array sensors and comparison to LoD values from ELISA methods. (c, d) Dose response obtained for different concentrations of MPO using graphene-coated nanoIDE-arrays and microIDE-arrays, respectively, and comparison of their performance with the ELISA-based approaches. 16 different devices were measured for each graph shown here.

References

Ahmad, Z.A., Yeap, S.K., Ali, A.M., Ho, W.Y., Alitheen, N.B., Hamid, M., 2012. scFv antibody: principles and clinical application. Clinical and Developmental Immunology 2012, 980250.
Ayyar, B.V., Hearty, S., O'Kennedy, R., 2010. Highly sensitive recombinant antibodies capable of reliably differentiating heart-type fatty acid binding protein from noncardiac isoforms. Analytical biochemistry 407(2), 165-171.
Azzazy, H.M., Pelsers, M.M., Christenson, R.H., 2006. Unbound free fatty acids and heart-type fatty acid-binding protein: diagnostic assays and clinical applications. Clinical chemistry 52(1), 19-29.
Baker, M., 2015. Blame it on the Antibodies. Nature 521, 274-276.
Balakumar, P., Maung, U.K., Jagadeesh, G., 2016. Prevalence and prevention of cardiovascular disease and diabetes mellitus. Pharmacological research 113(Pt A), 600-609.
Balasubramanian, K., Kern, K., 2014. 25th anniversary article: label-free electrical biodetection using carbon nanostructures. Adv. Mater. 26(8), 1154-1175.
Baldus, S., Heeschen, C., Meinertz, T., Zeiher, A.M., Eiserich, J.P., Münzel, T., Simoons, M.L., Hamm, C.W., 2003. Myeloperoxidase Serum Levels Predict Risk in Patients With Acute Coronary Syndromes. Circulation 108(12), 1440-1445.
Bellan, L.M., Wu, D., Langer, R.S., 2011. Current trends in nanobiosensor technology. Wiley interdisciplinary reviews. Nanomedicine and nanobiotechnology 3(3), 229-246.
Biju, V., 2014. Chemical modifications and bioconjugate reactions of nanomaterials for sensing, imaging, drug delivery and therapy. Chem. Soc. Rev. 43(3), 744-764.
Chatterjee, N.A., Singh, J.P., 2015. Novel Interventional Therapies to Modulate the Autonomic Tone in Heart Failure. JACC. Heart failure 3(10), 786-802.
Cong, C., Yu, T., 2014. Evolution of Raman G and G′(2D) modes in folded graphene layers. Physical Review B 89(23), 8.
Connolly, P., 1995. Clinical diagnostics opportunities for biosensors and bioelectronics. Biosensors and Bioelectronics 10, 1-6.
Damen, J.A., Hooft, L., Schuit, E., Debray, T.P., Collins, G.S., Tzoulaki, I., Lassale, C.M., Siontis, G.C., Chiocchia, V., Roberts, C., Schlussel, M.M., Gerry, S., Black, J.A., Heus, P., van der Schouw, Y.T., Peelen, L.M., Moons, K.G., 2016. Prediction models for cardiovascular disease risk in the general population: systematic review. Bmj 353, i2416.
Daniels, J.S.P., N., 2007. Label-Free Impedance Biosensors: Opportunities and Challenges. Electroanalysis 19(12), 1239-1257.
Das, A., Chakraborty, B., Sood, A.K., 2008. Raman spectroscopy of graphene on different substrates and influence of defects. Bull. Mater. Sci. 31(3), 579–584.
Esporcatte, R., Rey, H.C.V., Rangel, F.O.D., Rocha, R.M., de Mendonça Filho, H.T.F., Dohmann, H.F.R., Filho, F.M.A., 2007. Predictive value of myeloperoxidase to identify high risk patients admitted to the hospital with acute chest pain. Arq Bras Cardiol. 89(6), 377-384.
Fang, Y., 2015. Are label-free investigations the best approach to drug discovery? Future Med. Chem. 7(12), 1561-1564.
Ferrari, A.C., Basko, D.M., 2013. Raman spectroscopy as a versatile tool for studying the properties of graphene. Nat. Nanotechnol. 8, 235-246.
Goiffon, R.J., Martinez, S.C., Piwnica-Worms, D., 2015. A rapid bioluminescence assay for measuring myeloperoxidase activity in human plasma. Nature communications 6, 9.
Hinchet, R., Kim, S.W., 2015. Patient-Inspired Engineering and Nanotechnology. ACS Nano 9(8), 7742-7745.
Holliger, P., Hudson, P.J., 2005. Engineered antibody fragments and the rise of single domains. Nature biotechnology 23(9), 1126-1136.
Hozawa, A., Folsom, A.R., Sharrett, A., Chambless, L.E., 2007. Absolute and attributable risks of cardiovascular disease incidence in relation to optimal and borderline risk factors: Comparison of african american with white subjects—atherosclerosis risk in communities study. Archives of Internal Medicine 167(6), 573-579.

Huston, J.S., Levinson, D., Mudgett-Hunter, M., Tai, M.-S., Novotny, J., Margolies, M.N., Ridge, R.J., Bruccoleri, R.E., Haber, E., Crea, R., Oppermann, H., 1988. Protein engineering of antibody binding sites: Recovery of specific activity in an anti-digoxin single-chain Fv analogue produced in Escherichia coli. Proc. Natl. Acad. Sci. USA 85, 5879-5883.

Ishimura, S., Furuhashi, M., Watanabe, Y., Hoshina, K., Fuseya, T., Mita, T., Okazaki, Y., Koyama, M., Tanaka, M., Akasaka, H., Ohnishi, H., Yoshida, H., Saitoh, S., Miura, T., 2013. Circulating levels of fatty acid-binding protein family and metabolic phenotype in the general population. PloS one 8(11), 7.

Kaczynska, A., Pelsers, M.M., Bochowicz, A., Kostrubiec, M., Glatz, J.F., Pruszczyk, P., 2006. Plasma heart-type fatty acid binding protein is superior to troponin and myoglobin for rapid risk stratification in acute pulmonary embolism. Clinica chimica acta; international journal of clinical chemistry 371(1-2), 117-123.

Lanche, R., Pachauri, V., Law, J.K.Y., Munief, W.M., Wagner, P., Thoelen, R., Ingebrandt, S., 2015. Graphite oxide multilayers for device fabrication: Enzyme-based electrical sensing of glucose. Phys Status Solidi A 212(6), 1335-1341.

Lee, J.O., So, H.M., Jeon, E.K., Chang, H., Won, K., Kim, Y.H., 2008. Aptamers as molecular recognition elements for electrical nanobiosensors. Analytical and bioanalytical chemistry 390(4), 1023-1032.

Liang, Y., Chan, C.P.Y., Cheung, K.-y., Cautherley, G.W.H., Glatz, J.F.C., Renneberg, R., Zhu, J., 2011. CARDIODETECT RAPID TEST FOR THE DIAGNOSIS OF EARLY ACUTE MYOCARDIAL INFARCTION. Journal of Immunoassay and Immunochemistry 32(4), 342-352.

Lippi, G., Mattiuzzi, C., Cervellin, G., 2013. Critical review and meta-analysis on the combination of heart-type fatty acid binding protein (H-FABP) and troponin for early diagnosis of acute myocardial infarction. Clinical biochemistry 46(1-2), 26-30.

Luo, X., Davis, J.J., 2013. Electrical biosensors and the label free detection of protein disease biomarkers. Chem. Soc. Rev. 42(13), 5944-5962.

Ma, H., O'Kennedy, R., 2017. Recombinant Antibody Fragment Production. Methods 116, 23-33.

Mocatta, T.J., Pilbrow, A.P., Cameron, V.A., Senthilmohan, R., Frampton, C.M., Richards, A.M., Winterbourn, C.C., 2007. Plasma concentrations of myeloperoxidase predict mortality after myocardial infarction. Journal of the American College of Cardiology 49(20), 1993-2000.

Nicholls, S.J., Tang, W.H.W., Brennan, D., Brennan, M.-L., Mann, S., Nissen, S.E., Hazen, S.L., 2011. Risk Prediction with Serial Myeloperoxidase Monitoring in Patients with Acute Chest Pain. Clinical chemistry 57(12), 1762-1770.

O'Sullivan, C.K., 2002. Aptasensors--the future of biosensing? Analytical and bioanalytical chemistry 372(1), 44-48.

Oliveira Jr., O.N., Iost, R.M., Siqueira Jr., J.R., Crespilho, F.N., Caseli, L., 2014. Nanomaterials for diagnosis: challenges and applications in smart devices based on molecular recognition. ACS applied materials & interfaces 6(17), 14745-14766.

Otaki, Y., Watanabe, T., Takahashi, H., Hirayama, A., Narumi, T., Kadowaki, S., Honda, Y., Arimoto, T., Shishido, T., Miyamoto, T., Konta, T., Shibata, Y., Fukao, A., Daimon, M., Ueno, Y., Kato, T., Kayama, T., Kubota, I., 2014. Association of Heart-Type Fatty Acid-Binding Protein with Cardiovascular Risk Factors and All-Cause Mortality in the General Population: The Takahata Study. PloS one 9(5), 10.

Pachauri, V.I., S., 2016. Biologically sensitive field-effect transistors: from ISFETs to NanoFETs. Essays in biochemistry 60(1), 81-90.

Park, K., Ryu, S., 2015. Direction-controlled chemical doping for reversible G-phonon mixing in ABC trilayer graphene. Scientific Report 5, 8.

Pickup, J.C., 1985. Biosensors: A clinical Perspective. The Lancet, 817-820.

Rani, D., Pachauri, V., Mueller, A., Vu, X.T., Nguyen, T.C., Ingebrandt, S., 2016. On the Use of Scalable NanoISFET Arrays of Silicon with Highly Reproducible Sensor Performance for Biosensor Applications. ACS Omega 1(1), 84-92.

Savic-Radojevic, A., Pljesa-Ercegovac, M., Matic, M., Simic, D., Radovanovic, S., Simic, T., 2017. Chapter Four - Novel Biomarkers of Heart Failure. In: Gregory, S.M. (Ed.), Advances in Clinical Chemistry, pp. 93-152. Elsevier.

Schroeder, F., Jolly, C.A., Cho, T.-H., Frolov, A., 1998. Fatty acid binding protein isoforms: structure and function. Chemistry and Physics of Lipids 92, 1-25.
Shearer, C.J., Slattery, A.D., Stapleton, A.J., Shapter, J.G., Gibson, C.T., 2016. Accurate thickness measurement of graphene. Nanotechnology 27(12), 10pp.
Spain, E., Gilgunn, S., Sharma, S., Adamson, K., Carthy, E., O'Kennedy, R., Forster, R.J., 2016. Detection of prostate specific antigen based on electrocatalytic platinum nanoparticles conjugated to a recombinant scFv antibody. Biosensors and Bioelectronics 77, 759-766.
Steg, P.G., James, S.K., Atar, D., Badano, L.P., Blomstrom-Lundqvist, C., Borger, M.A., Di Mario, C., Dickstein, K., Ducrocq, G., Fernandez-Aviles, F., Gershlick, A.H., Giannuzzi, P., Halvorsen, S., Huber, K., Juni, P., Kastrati, A., Knuuti, J., Lenzen, M.J., Mahaffey, K.W., Valgimigli, M., van 't Hof, A., Widimsky, P., Zahger, D., 2012. ESC Guidelines for the management of acute myocardial infarction in patients presenting with ST-segment elevation. European Heart Journal 33(20), 2569-2619.
Wang, J., Tan, G.J., Han, L.N., Bai, Y.Y., He, M., Liu, H.B., 2017. Novel biomarkers for cardiovascular risk prediction. Journal of geriatric cardiology : JGC 14(2), 135-150.
Wilkins, E., Wilson, L., Wickramasinghe, K., Bhatnagar, P., Rayner, M., Townsend, N., Leal, J., Luengo-Fernandez, R., Burns, R., 2017. European Cardiovascular Disease Statistics 2017 edition. European Heart Network.
Wodzigl, K.W.H., Pelsersl, M.M.A.L., van der Vussel, G.J., Roos, W., Glatz, J.F.C., 1997. One-step enzyme-linked immunosorbent assay (ELISA) for plasma fatty acid-binding protein. Ann Clin Biochem 34, 263-268.
Yu, H.K., Balasubramanian, K., Kim, K., Lee, J.-L., Maiti, M., Ropers, C., Krieg, J., Kern, K., Wodtke, A.M., 2014. Chemical Vapor Deposition of Graphene on a “Peeled-Off” Epitaxial Cu(111) Foil: A Simple Approach to Improved Properties. ACS Nano 8(8), 8636–8643.

Highlights:

1. First report on the high-performance label-free electrical bioassay for fatty-acid binding protein and myeloperoxidase (cardiac biomarkers) in physiological saline using specially engineered single-chain fragment variable (scFv) antibodies as receptors
2. Electrical bioassay widely covering the clinically relevant ranges.
3. Highly reproducible sensor characteristics emanating from the novel design of electrical transducer platform of graphene-coated interdigitated electrode arrays.
4. Impressive performance of the sensor platform expected to go further for clinical validation studies.